

DTU candidate field models for IGRF-12 and the CHAOS-5 geomagnetic field model

Finlay, Chris; Olsen, Nils; Tøffner-Clausen, Lars

Published in:
Earth, Planets and Space

Link to article, DOI:
[10.1186/s40623-015-0274-3](https://doi.org/10.1186/s40623-015-0274-3)

Publication date:
2015

Document Version
Peer reviewed version

[Link back to DTU Orbit](#)

Citation (APA):
Finlay, C., Olsen, N., & Tøffner-Clausen, L. (2015). DTU candidate field models for IGRF-12 and the CHAOS-5 geomagnetic field model. *Earth, Planets and Space*, 67(114). DOI: 10.1186/s40623-015-0274-3

DTU Library Technical Information Center of Denmark

General rights

Copyright and moral rights for the publications made accessible in the public portal are retained by the authors and/or other copyright owners and it is a condition of accessing publications that users recognise and abide by the legal requirements associated with these rights.

- Users may download and print one copy of any publication from the public portal for the purpose of private study or research.
- You may not further distribute the material or use it for any profit-making activity or commercial gain
- You may freely distribute the URL identifying the publication in the public portal

If you believe that this document breaches copyright please contact us providing details, and we will remove access to the work immediately and investigate your claim.

RESEARCH

DTU candidate field models for IGRF-12 and the CHAOS-5 geomagnetic field model

Christopher C. Finlay^{*}, Nils Olsen
and Lars Tøffner-Clausen

^{*}Correspondence:

cfinlay@space.dtu.dk

Division of Geomagnetism, DTU Space, Technical University of Denmark, Diplomvej, 371, Kongens Lyngby, Denmark
Full list of author information is available at the end of the article

Abstract

We present DTU's candidate field models for IGRF-12 and the parent field model from which they were derived, CHAOS-5. Ten months of magnetic field observations from ESA's *Swarm* mission, together with up-to-date ground observatory monthly means, were used to supplement the data sources previously used to construct CHAOS-4. The internal field part of CHAOS-5, from which our IGRF-12 candidate models were extracted, is time-dependent up to spherical harmonic degree 20 and involves sixth order splines with a 0.5 yr knot spacing. In CHAOS-5, compared with CHAOS-4, we update only the low degree internal field model (degrees 1 to 24) and the associated external field model. The high degree internal field (degrees 25 to 90) is taken from the same model CHAOS-4h, based on low amplitude CHAMP data, that was used in CHAOS-4 ([Olsen *et al.*, 2014](#)).

We find that CHAOS-5 is able to consistently fit magnetic field data from six independent low Earth orbit satellites: Ørsted, CHAMP, SAC-C and the three *Swarm* satellites (A, B and C). It also adequately describes the secular variation measured at ground observatories. CHAOS-5 thus contributes to an initial validation of the quality of the *Swarm* magnetic data, in particular demonstrating that Huber weighted rms model residuals to *Swarm* vector field data are lower than those to Ørsted and CHAMP vector data (when either one or two star cameras were operating). CHAOS-5 shows three pulses of secular acceleration at the core surface over the past decade; the 2006 and 2009 pulses have previously been documented, but the 2013 pulse has only recently been identified. The spatial signature of the 2013 pulse at the core surface, under the Atlantic sector where it is strongest, is well correlated with the 2006 pulse, but anti-correlated with the 2009 pulse.

Keywords: Geomagnetism; Field Modelling; IGRF; *Swarm*

1 Introduction

In May 2014 the IAGA task force responsible for IGRF-12 requested candidate geomagnetic reference field models [main field (MF) for epochs 2010.0, 2015.0 and predictive secular variation (SV) for 2015.0-2020.0] to be submitted by 1st October 2014. This article describes in detail the candidate models submitted by DTU Space and the time-dependent parent model from which they were derived, called CHAOS-5.

Geomagnetic field modellers producing candidate models for IGRF-12 were in the fortunate position that ESA launched the *Swarm* satellite constellation, whose aim is to carry out the best ever survey of the Earth's magnetic field, in November 2013.

In parallel with ongoing calibration and validation efforts, ESA promptly released L1b magnetic field data to the scientific community by May 2014. *Swarm* data were crucial to the DTU candidate models presented below. We therefore describe the selection, processing, and modelling of the *Swarm* data in some detail. In addition to data from *Swarm*, we used data from previous satellite missions (Ørsted, CHAMP and SAC-C), along with ground-observatory data kindly provided and checked by the British Geological Survey ([Macmillan and Olsen, 2013](#)).

CHAOS-5, the parent model for the IGRF-12 candidates reported here, is the latest update of the CHAOS field model series ([Olsen *et al.*, 2006, 2009, 2010, 2014](#)). The crucial aspects of this model are a time-dependent model of the large-scale internal field, a static model of the smaller-scale internal field, a parameterization of the large-scale external field in both SM co-ordinates (with time-dependence parameterized by a disturbance index) and GSM co-ordinates, and a co-estimation of the Euler angles used for the rotation of the three-component vector field from the magnetometer frame to the star camera frame.

The main improvement of CHAOS-5 over CHAOS-4 is its use of 10 months of *Swarm* data, as well as more recent ground observatory data. The modelling technique and data selection closely follows that previously described by [Olsen *et al.* \(2014\)](#). CHAOS-5 is similar to the IGRF parent models produced by a number of other teams (for example [Maus *et al.*, 2010](#); [Rother *et al.*, 2013](#); [Thomson *et al.*, 2010](#)) in not explicitly modelling the ionospheric field, in contrast to the more sophisticated comprehensive modelling approach ([Sabaka *et al.*, 2015](#); [Thébault *et al.*, 2015](#)). Instead data selection for CHAOS-5 is limited to dark-region data from geomagnetically quiet times (when ionospheric currents are weak, at least at non-polar latitudes), in an effort to isolate as best as possible the field of internal origin.

In section 2 we provide more details concerning the data selection and processing used in the construction of CHAOS-5. Section 3 gives a brief description of our model parameterization and section 4 describes the procedure for model estimation, including the chosen temporal regularization. Differences between CHAOS-5 and CHAOS-4 are summarized in Table 1. Details concerning the extraction of the IGRF-12 candidate models are given in section 5. In section 6, results from CHAOS-5 are presented, including its fit to ground observatory and satellite data, and the evolution of its model SV, which is, of course, relevant regarding the predictive SV. The time evolution of the secular acceleration (SA) in CHAOS-5 is also described and an interesting new SA pulse at the core surface in 2013 is documented. Finally, a summary and the conclusions of the study are presented in section 7.

2 Data

2.1 Satellite Data

Dark-region data from geomagnetically quiet times, suitable for use within the CHAOS field modelling scheme, have been selected. In particular the following selection criteria, previously used in the CHAOS-4 model ([Olsen *et al.*, 2014](#)), have again been employed:

- 1) Dark regions only (sun at least 10° below the horizon);
- 2) Strength of the magnetospheric ring-current, estimated using the *RC*-index ([Olsen et al., 2014](#)), was required to change by at most 2 nT/hr;
- 3) Three vector components of the magnetic field were taken for quasi-dipole (QD) latitudes equatorward of $\pm 55^\circ$, while scalar field (intensity) data only were used for higher QD latitudes or when attitude data were not available;
- 4) Geomagnetic activity at non-polar latitudes (equatorward of $\pm 55^\circ$ QD latitude) was sufficiently low, such that the index $Kp \leq 2^0$;
- 5) Poleward of $\pm 55^\circ$ QD latitude, scalar data were only selected when the merging electric field at the magnetopause $E_m = 0.33v^{4/3}B_t^{2/3}\sin^{8/3}(|\Theta|/2)$, where v is the solar wind speed, $B_t = \sqrt{B_y^2 + B_z^2}$ is the magnitude of the Interplanetary Magnetic Field in the $y-z$ plane in GSM coordinates and $\Theta = \arctan(B_y/B_z)$ ([Newell et al., 2007](#)), was sufficiently small. More precisely, the weighted average over the preceding one hour, $E_{m,12} \leq 0.8$ mV/m.

All satellite data are further weighted proportional to $\sin \theta$ (where θ is geographic co-latitude) to simulate an equal-area distribution. The treatment and processing of Ørsted, CHAMP and SAC-C data generally follows that previously described for the CHAOS-4 field model ([Olsen et al., 2014](#)). Fig. 1 presents the total number of non-polar magnetic satellite observations used each month in deriving the CHAOS-5 model. Note that because there are three *Swarm* satellites, and because their data are selected in the same manner, there were a relatively large number of data available since the launch of *Swarm* in November 2013.

From ESA's *Swarm* satellite trio, we used the operational L1b data product Mag-L, for the 10 months 26th November 2013 to 25th September 2014, release 0302 when available, otherwise release 0301. Data were selected from the three satellites, *Swarm* A, B and C at 60 second intervals unless Flags_B=255 or Flags_q= 255, which specifies non-valid magnetometer or attitude data, (see [Olsen et al., 2013](#), for a more detailed description of the L1b products and related flags). We manually rejected *Swarm* A data from 29th - 30th January 2014, and 6th February 2014 as well as *Swarm* C data from 25th - 26th March 2014 and 4th, 8th and 11th April 2014 when notably large outliers were identified, likely a result of specific manoeuvres that were carried out on these days. In addition, gross outliers were excluded by requiring that all vector field components be within 500 nT (and the scalar field within 100 nT) of the predictions of a preliminary field model, CHAOS-4plus.V4, that we constructed using the satellite and ground observatory data available in August 2014. The Vector Field Magnetometer (VFM) data were also slightly re-scaled, point-by-point isotropically forcing their scalar value to agree with the Absolute Scalar Magnetometer (ASM) data. This was a simple attempt to make the ASM and VFM datasets more consistent, in the absence of a suitable vector field correction at the time of model determination in September 2014. Tests showed the impact of this scaling on magnetic field models was however small, in part because data from sunlit regions (which have larger ASM-VFM differences, see [Lesur et al., 2015](#)) were not selected. At polar latitudes only ASM scalar data were used. In all we used $3 \times 53,137$ (17,485) vector data (scalar data) from *Swarm*

A, $3 \times 53,253$ (17,744) from *Swarm* B, and $3 \times 49,984$ (16,697) from *Swarm* C respectively. The altitude of the three *Swarm* satellites versus time, and the coverage of the selected data as a function of latitude and time is presented in Fig. 2.

2.2 Observatory data

Annual differences of revised observatory monthly means (*Olsen et al., 2014*) for the time interval January 1997 to September 2014 were used as additional observational constraints on the SV. Revised monthly means were derived from the hourly mean values of 159 observatories (locations shown in Fig. 3) which have been carefully checked for trends, spikes and other errors (*Macmillan and Olsen, 2013*). The observatory data were rotated from geodetic to geographic components. Prior to producing monthly means by a robust method based on Huber weights (*Huber, 1964*), we removed estimates of the ionospheric (plus induced) field as predicted by the CM4 model (*Sabaka et al., 2004*) and the large-scale magnetospheric (plus induced) field, as predicted by the preliminary field model CHAOS-4plus_V4. After taking annual differences, this resulted in 21,733 values of the first time derivative of the vector field components, $dB_r/dt, dB_\theta/dt, dB_\phi/dt$ with the distribution in time shown in the bottom panel of Fig. 3. We emphasize that CM4-based estimates of the ionospheric field were removed only from the hourly mean observatory data during the derivation of revised monthly means (since data from all local times were used) and they were not removed from the dark-region satellite data used.

3 Model parameterization

The parametrization of the CHAOS-5 field model follows closely that of previous versions in the CHAOS model series (*Olsen et al., 2006, 2009, 2010, 2014*). We assume measurements take place in a region free from electric currents, in which case the vector magnetic field \mathbf{B} may be described by a potential such that $\mathbf{B} = -\nabla V$. The magnetic scalar potential $V = V^{\text{int}} + V^{\text{ext}}$ consists of V^{int} , describing internal (core and lithospheric) sources, and V^{ext} , describing external (mainly magnetospheric) sources and their Earth-induced counterparts. Both internal and external parts are expanded in spherical harmonics. The CHAOS-5 model thus consists of spherical harmonic coefficients together with sets of Euler angles for rotating the satellite vector field readings from the magnetometer frame to the star camera frame.

Considering first the internal field, we work in an Earth-Centered-Earth-Fixed (ECEF) coordinate system using a spherical harmonic expansion

$$V^{\text{int}} = a \sum_{n=1}^{N_{\text{int}}} \sum_{m=0}^n (g_n^m \cos m\phi + h_n^m \sin m\phi) \left(\frac{a}{r}\right)^{n+1} P_n^m(\cos \theta) \quad (1)$$

where $a = 6371.2$ km is a reference radius, (r, θ, ϕ) are geographic spherical polar coordinates, $P_n^m(\cos \theta)$ are the Schmidt semi-normalized associated Legendre functions, $\{g_n^m, h_n^m\}$ are the Gauss coefficients describing internal sources, and N_{int} is the maximum degree and order of the internal expansion. The internal coefficients

144 $\{g_n^m(t), h_n^m(t)\}$ up to $n = 20$ are time-dependent; this dependence is described by
 145 order 6 B-splines (De Boor, 2001) with a 6-month knot separation and five-fold
 146 knots at the endpoints $t = 1997.0$ and $t = 2015.0$. Internal coefficients for degrees
 147 21 and above are static, a maximum degree of 80 was used during the derivation of
 148 the new model for the low degree field (CHAOS-5l, where ‘l’ denotes low degrees)
 149 described here.

150
 151 Regarding the external field, we represent the near magnetospheric sources, e.g.,
 152 magnetospheric ring current, by a spherical harmonic expansion in *Solar Magnetic*
 153 (*SM*) coordinates (up to $n = 2$, with a special treatment of the $n = 1$ terms).
 154 Regarding remote magnetospheric sources, e.g., magnetotail and magnetopause
 155 currents, we use a spherical harmonic expansion in *Geocentric Solar Magnetospheric*
 156 (*GSM*) coordinates (also up to $n = 2$, but restricted to order $m = 0$):

$$\begin{aligned}
 V^{\text{ext}} &= a \sum_{n=1}^2 \sum_{m=0}^n (q_n^m \cos mT_d + s_n^m \sin mT_d) \left(\frac{r}{a}\right)^n P_n^m(\cos \theta_d) \\
 &+ a \sum_{n=1}^2 q_n^{0,\text{GSM}} R_n^0(r, \theta, \phi)
 \end{aligned} \tag{2}$$

where θ_d and T_d are dipole co-latitude and dipole local time. The degree-1 coefficients in *SM* coordinates are time-dependent and are further expanded as

$$q_1^0(t) = \hat{q}_1^0 \left[\epsilon(t) + \iota(t) \left(\frac{a}{r}\right)^3 \right] + \Delta q_1^0(t) \tag{3a}$$

$$q_1^1(t) = \hat{q}_1^1 \left[\epsilon(t) + \iota(t) \left(\frac{a}{r}\right)^3 \right] + \Delta q_1^1(t) \tag{3b}$$

$$s_1^1(t) = \hat{s}_1^1 \left[\epsilon(t) + \iota(t) \left(\frac{a}{r}\right)^3 \right] + \Delta s_1^1(t) \tag{3c}$$

157 where the terms in brackets describe the contributions from the magnetospheric
 158 ring-current and its Earth-induced counterpart as estimated by the RC index (Olsen
 159 et al., 2014), $RC(t) = \epsilon(t) + \iota(t)$. We co-estimate the time-independent regression
 160 factors $\hat{q}_1^0, \hat{q}_1^1, \hat{s}_1^1$ and the time-varying “RC baseline corrections” $\Delta q_1^0, \Delta q_1^1$ and Δs_1^1
 161 in bins of 5 days (for Δq_1^0) and 30 days (for $\Delta q_1^1, \Delta s_1^1$), respectively. These allow for
 162 differences between the ground-based estimate of the degree 1 external magnetic
 163 signal (the RC index) and that inferred from low-Earth orbit satellites.

164
 165 In addition to the above spherical harmonic coefficients, we co-estimate the Euler
 166 angles describing the rotation between the vector magnetometer frame and the star
 167 camera frame. For Ørsted this yields two sets of Euler angles (one for the period
 168 before 24 January 2000 when the onboard software of the star camera was updated
 169 and one for the period after that date), while for CHAMP and each *Swarm* satellite
 170 we solve for Euler angles in bins of 10 days.

171
 172 The new model described here, derived specifically to produce candidate mod-
 173 els for IGRF-12, is essentially an update of the model CHAOS-4l including 10

months of *Swarm* data and the latest annual differences of observatory revised month means. We refer to this new parent model as CHAOS-5l. It involves time-dependent terms (for degrees $n = 1 - 20$, 18,040 coefficients) and static terms (for $n = 21 - 80$, 6120 coefficients) together resulting in a total of 24,160 internal Gauss coefficients. The total number of external field parameters is 1,301, which is the sum of 5 SM terms (q_2^m, s_2^m for $n = 2$), 3 RC regression coefficients $\tilde{q}_1^0, \tilde{q}_1^1, \tilde{s}_1^1$, 2 GSM coefficients ($q_n^{1,\text{GSM}}, q_n^{2,\text{GSM}}$), 949 baseline corrections Δq_1^0 and 2×171 baseline corrections $\Delta q_1^1, \Delta s_1^1$. Considering the Euler angles for the Ørsted, CHAMP and the *Swarm* satellites yields an additional $3 \times (2 + 366 + 94) = 1,386$ model parameters. This finally results in a total of $24,160 + 1,301 + 1,386 = 26,847$ model parameters to be estimated.

4 Model estimation and regularization

The model parameters described above for CHAOS-5l were estimated from 753,996 scalar data and $3 \times 741,440$ vector data by means of a regularized *Iteratively Reweighted Least-Squares* algorithm using Huber weights, minimizing the cost function

$$\mathbf{e}^T \underline{\underline{C}}^{-1} \mathbf{e} + \lambda_3 \mathbf{m}^T \underline{\underline{\Lambda}}_3 \mathbf{m} + \lambda_2 \mathbf{m}^T \underline{\underline{\Lambda}}_2 \mathbf{m} \quad (4)$$

where \mathbf{m} is the model vector, the residuals vector $\mathbf{e} = \mathbf{d}_{\text{obs}} - \mathbf{d}_{\text{mod}}$ is the difference between the vector of observations \mathbf{d}_{obs} and the vector of model predictions \mathbf{d}_{mod} , and $\underline{\underline{C}}$ is the data error covariance matrix.

In the data error covariance matrix $\underline{\underline{C}}$, anisotropic errors due to attitude uncertainty (Holme and Bloxham, 1996) are considered for the vector field satellite data. A-priori data error variances for the scalar field were assumed to be 2.5 nT for Ørsted and 2.2 nT for CHAMP and *Swarm*, while the attitude uncertainties were allocated as in CHAOS-4 (Olsen et al., 2014), but with a pointing uncertainty of 10 arcseconds for *Swarm* vector field data.

$\underline{\underline{\Lambda}}_3$ and $\underline{\underline{\Lambda}}_2$ are block diagonal regularization matrices penalizing the squared values of the third, respectively second, time derivatives of the radial field B_r at the core surface. $\underline{\underline{\Lambda}}_3$ involves integration over the full timespan of the model while $\underline{\underline{\Lambda}}_2$ involves evaluating the second time derivative only at the model endpoints $t = 1997.0$ and 2015.0 . The parameters λ_3 and λ_2 control the strength of the regularization applied to the model time-dependence during the entire modelled interval and at the endpoints, respectively. We tested several values for these parameters and finally selected $\lambda_3 = 0.33 \text{ (nT/yr}^3\text{)}^{-2}$ (the same as used in CHAOS-4l) and $\lambda_2 = 100 \text{ (nT/yr}^2\text{)}^{-2}$ (a stronger endpoint constraint than used in CHAOS-4l). In addition, all zonal terms were treated separately (in CHAOS-4l only the axial dipole was treated separately), with λ_3 increased to $100 \text{ (nT/yr}^3\text{)}^{-2}$, since we found these internal field components were being more strongly perturbed by (i) unmodelled external field fluctuations and (ii) short-comings in the data-coverage due to lack of data in the summer polar region. The regularization parameters were chosen

from a series of experiments, relying on comparisons to the SV recorded at ground observatories.

Since both scalar data and Huber weights are involved, the cost function depends nonlinearly on the model parameters. The solution to the minimization problem was therefore obtained iteratively using a Newton-type algorithm. The starting model was a single epoch model with linear SV centered on 2010.0. The final model was obtained after 6 iterations, by which point sufficient convergence was obtained with misfits converging to better than 0.01 nT and the Euclidean norm of the model change in the final iteration less than 0.005% that of the model itself.

The complete CHAOS-5 field model was obtained in a final step by combining the spherical harmonic coefficients of new model CHAOS-5l with the previous CHAOS-4h model (*Olsen et al., 2014*), which in September 2014 was our best model for the high degree lithospheric field. The transition between these models was implemented at $n = 24$ as for CHAOS-4. The various differences between CHAOS-5 and CHAOS-4 are collected for reference in Table 1. Note that the model statistics reported below are those for CHAOS-5l, the parent model from which our IGRF-12 candidate models were extracted.

5 Derivation of candidate models for IGRF-12

IGRF-12 candidates were extracted from the parent model CHAOS-5l as follows:

- **DGRF, epoch 2010.0**

The parent model CHAOS-5l, with its spline-based time-dependence, was evaluated at epoch 2010.0 and the internal spherical harmonic coefficients up to degree and order 13 output to 0.01 nT.

- **IGRF, epoch 2015.0**

The parent model CHAOS-5l, with its spline-based time-dependence was evaluated at epoch 2014.75, the end of the month when the last input satellite data were available to constrain the model. The resulting coefficients were then propagated forward to epoch 2015.0, using the linear SV evaluated from CHAOS-5l in epoch 2014.0 (as in our SV candidate, to avoid spline-model end effects) as follows:

$$g_n^m(t = 2015.0) = g_n^m(t = 2014.75) + 0.25 \cdot \dot{g}_n^m(t = 2014.0) \quad (5)$$

Here g_n^m represents each of the Gauss coefficients $\{g_n^m, h_n^m\}$ while \dot{g}_n^m represents the SV coefficients $\{\dot{g}_n^m, \dot{h}_n^m\}$ in nT/yr. The resulting internal spherical harmonic coefficients for the internal field in epoch 2015.0 up to degree and order 13 were output to 0.01 nT.

- **Predicted average SV, 2015.0 to 2020.0**

Since there can be spline-model end effects in the secular acceleration (SA), we

evaluated the SV from CHAOS-5l at epoch 2014.0, rather than in 2015.0, and did not attempt any extrapolation. These end effects are essentially due to the lack of ‘future’ data for constraining the SV and SA at the model endpoint, and because SV estimates based on annual differences of ground observatory monthly means are available only up to 6 months before the latest available ground observatory data. It should also be noted that the SV in a spline-based model such as CHAOS-5l at a particular epoch is not the true instantaneous SV, but a weighted time-average, with the amount of time-averaging varying with spherical harmonic degree according to the imposed regularization.

The SV spherical harmonic coefficients (first time derivative of the spline model) for the internal field in epoch 2014.0, up to degree and order 8 were then output to 0.01 nT/yr. We also provided SV predictions to degree and order 13 as a test secular variation model.

No uncertainty estimates were provided with our candidate models, since we are unable to calculate satisfactory estimates. The largest errors are likely biases caused by unmodelled sources ([Sabaka et al., 2015](#)) which cannot be assessed using a formal model error covariance matrix, or by constructing models using the same technique from independent datasets.

6 Results and discussion

6.1 Fit to satellite data

Statistics for the misfit between the CHAOS-5l parent field model and the observations used to derive it are collected in Table 2, using the (B_B, B_\perp, B_3) notation of [Olsen \(2002\)](#) that is relevant when describing anisotropic pointing errors. The weighted rms misfits to the Ørsted, CHAMP and SAC-C data are similar to those found previously for CHAOS-4l. Regarding the *Swarm* data, the Huber weighted rms misfits to scalar intensity data ($F_{\text{nonpolar}} + B_B$) of 2.09 nT for *Swarm* A, 2.07 nT for *Swarm* B and 2.09 nT for *Swarm* C are very similar to that found for the CHAMP data, 2.07 nT, considering all 10 years of operation. However the misfit to the other two vector field components (B_\perp and B_3) was approximately 0.5 nT lower for *Swarm* data compared to CHAMP data (note the distinction between B_\perp and B_3 is arbitrary for *Swarm*, while CHAMP data with either one or two star cameras operating have been considered. This difference mapped into lower misfits to *Swarm* data in the B_r and B_θ geocentric components, (e.g., the Huber weighted rms misfit for B_r was 2.77 nT for CHAMP compared to 1.83 nT, 1.99 nT and 1.93 nT for *Swarm* A, B, C respectively).

The residuals between CHAOS-5l and the *Swarm* magnetic field data, show the expected trends as function of geomagnetic latitude (see Fig. 4, left panel), with the scalar residuals being much larger in the polar region and minimum close to ± 35 degrees geomagnetic latitude, where the perturbations due to unmodelled ring current fluctuations are perpendicular to the dipole-dominated main field. The Huber weighted residuals as a function of time for *Swarm* A, B, and C at this geomagnetic

latitude (± 35 degrees) are presented in Fig. 4, right panel. Residuals are usually less than ± 5 nT for all three satellites at this location, with similar trends seen for each satellite.

6.2 Fit to observatory monthly means

The fit of CHAOS-5l to annual differences of observatory monthly means is similar to that obtained for the previous CHAOS-4l model, with the rms Huber weighted misfits for dB_r/dt , dB_θ/dt and dB_ϕ/dt of 3.91 nT/yr, 3.83 nT/yr and 3.12 nT/yr respectively. Examples of comparisons between the SV predicted by CHAOS-5l and SV estimates from annual differences of monthly means at selected observatories are presented in Fig. 5. CHAOS-5l succeeds in reproducing the SV trends on timescales of two years and longer at these observatories. The SV obtained from CHAOS-5l thus appears reasonable, at least up to the time of the latest available observatory available SV estimates, from early 2014 (using annual differences of monthly means up to August 2014). There is a clear improvement in the SV predicted by the CHAOS-5 compared to that predicted by CHAOS-4 in 2013 and 2014 (e.g., dB_r/dt at HER, dB_θ/dt at NGK, KAK, dB_ϕ/dt at HON, HER).

6.3 Time-dependence of secular variation coefficients

The time evolution of the SV in CHAOS-5l for degrees 1 to 8 is presented in Fig. 6, with the SV from CHAOS-4l again shown for reference. The two models agree well until approximately 2013, after which the SV from CHAOS-4l diverges from that of CHAOS-5l, particularly in the lowest degrees which were least regularized. Note that penalization of SA at the model endpoints was imposed more strongly in CHAOS-5l, hence its SV is close to constant near the ends of the model timespan. In addition the zonal terms ($m=0$), which showed some possibly spurious SV trends close to the endpoints in CHAOS-4 (e.g., in dg_1^0/dt , dg_2^0/dt) were damped more heavily in CHAOS-5l.

6.4 Spectral properties of DTU IGRF-12 candidate models

The power spectra of the DTU candidate MF and SV models for IGRF-12 are presented in Fig. 7, along with spectra of comparable models from IGRF-11, the MF in 2010.0, and the predicted SV for 2015.0 to 2020.0. The spectra of our IGRF-12 MF candidates are very similar to the IGRF-11 MF in 2010.0. The spectra of the difference between our DGRF-2010 candidate and IGRF-2015 candidate, divided by 5 to get a change per year is also very close to the spectrum of the predicted SV for 2010.0 to 2015.0 from IGRF-11 (Finlay *et al.*, 2010). In comparison the spectrum of our new SV candidate for 2015.0 to 2020.0 contains slightly more power at degrees 3 to 5, but is otherwise similar.

6.5 Rationale for choice of SV candidate

The construction and evaluation of SV candidates has long been considered the most challenging aspect of producing a new IGRF generation (Lowes, 2000). Here,

we derived our IGRF-12 SV candidate taking the position that it is not yet possible to reliably predict future SA events (for example related to geomagnetic jerks) since prognostic forward models capturing the relevant core physics on short time scales are not yet available. We therefore take our estimate of the current SV to be our prediction of the SV for 2015.0 to 2020.0, essentially assuming no average SA or equivalently that the SA will average to zero over the upcoming five years. As discussed above we take the SV from 2014.0 in our spline model as our estimate of the present SV, to avoid problems related to spline model end-effects.

6.6 Secular acceleration pulses in 2006, 2009 and 2013

Pulses of SA at the core surface have been identified in the past decade ([Chulliat *et al.*, 2010](#)), primarily using data collected by the CHAMP satellite. They are thought to underlie localized rapid secular variation events observed at Earth's surface ([Lesur *et al.*, 2008](#); [Olsen and Manda, 2008](#)) and the well-known geomagnetic jerks seen in ground observatory data ([Chulliat *et al.*, 2010](#)). Previous studies have highlighted two pulses in 2006 and 2009 in opposite directions ([Chulliat and Maus, 2014](#); [Olsen *et al.*, 2014](#)). These SA pulses are clearly evident when plotting the time evolution of the SA power integrated over the core surface, as given by

$$S_A = \sum_{n=1}^{N_{SA}} (n+1) \left(\frac{c}{a}\right)^{2n+4} \sum_m (\ddot{g}_n^m)^2 + (\ddot{h}_n^m)^2, \quad (6)$$

for example, as shown in Fig 8. Here, we take $c = 3480\text{km}$ to be the radius of the core surface, $\{\ddot{g}_n^m, \ddot{h}_n^m\}$ are the Gauss coefficients for the SA, evaluated from the 6th order spline model, and we have chosen the degree of truncation $N_{SA} = 8$, to reflect those degrees in which we see well resolved time-dependence of the SV. In Fig 8 we plot $S_A(t)$ from both CHAOS-4 and the new CHAOS-5 model. They agree rather well up until 2011, although we find slightly more SA power in the 2009 pulse in CHAOS-5. The major difference between CHAOS-4 and CHAOS-5 is a strong SA pulse seen in 2013 in CHAOS-5. There was possibly already weak evidence for a pulse around 2013 in CHAOS-4, but the sparsity of satellite data in this model after 2010, and the closeness of the pulse to the model endpoint, made interpretation of this feature difficult. Evidence for the 2013 pulse was first presented at the 3rd *Swarm* Science Meeting (Copenhagen, June 2014) by two independent teams. Chulliat, Alken and Maus, (see [Chulliat *et al.*, 2015](#)), highlighted evidence derived from DMSP satellite data, while the present authors showed results from a preliminary version of CHAOS-5.

[Chulliat and Maus \(2014\)](#) pointed out that the dominant signatures of the 2006 and 2009 pulses in the radial SA at the core-mantle boundary, found in the low latitude Atlantic sector, are essentially anti-correlated. In CHAOS-5 we find that for the new pulse in 2013, the radial SA signature in the Atlantic sector is again correlated with the 2006 pulse and anti-correlated with the 2009 pulse, as shown in Fig. 9. A detailed discussion of this point, and corroborating evidence obtained from the DMSP satellites, is given by [Chulliat *et al.* \(2015\)](#).

A striking example of the oscillatory core surface SV that now requires an explanation is that the strongest feature in the radial SA under the eastern edge of Brazil was negative in 2006, positive in 2009, and negative again in 2013. [Gillet *et al.* \(2015\)](#) have proposed that such events can be explained by oscillations in the non-zonal (i.e. non-axisymmetric) part of the azimuthal (east-west) quasi-geostrophic core flow at low latitudes. [Chulliat *et al.* \(2015\)](#) suggest an alternative idea that fast equatorial MHD waves in a stratified layer at the top of the core may be responsible. The identification of the 2013 pulse in CHAOS-5 opens the door to further detailed study of such hypotheses. The occurrence of SA pulses in 2006.2, 2009.2 and 2013.9 also leads us to wonder whether the next pulse, expected to have the same polarity as the 2009 event, might occur around 2016, before the end of the nominal *Swarm* mission. Since *Swarm* should be providing high quality magnetic field measurements with unprecedented space-time coverage throughout this period, it promises to be an exciting opportunity to characterize a SA pulse in great detail.

7 Conclusions

We have presented the CHAOS-5 geomagnetic field model, including the parent model CHAOS-5l from which DTU's candidate field models for IGRF-12 were derived. Details of the magnetic data used to construct CHAOS-5 (including their selection and processing) have been documented, with a focus on data from ESA's *Swarm* satellite constellation. The CHAOS-5 model parameterization and estimation scheme has been reported, and details given concerning how the candidate field models for IGRF-12 were extracted.

We find acceptable misfits of CHAOS-5 to both ground observatory and *Swarm* data in 2014, and no evidence of unreasonable model oscillations or spurious trends. CHAOS-5 thus provides a consistent representation of magnetic data from six independent satellites (\O rsted , CHAMP, SAC-C and *Swarm* A, B, C), as well as ground observatory data, between 1999 and 2015. The Huber weighted rms misfit of the CHAOS-5 model to the *Swarm* vector field data is found to be lower than the Huber weighted rms misfit to the \O rsted and CHAMP vector field data (where either 1 or 2 star cameras were operating), for example considering the radial field component, Huber weighted rms misfits of 1.83nT, 1.99nT and 1.93 nT to *Swarm* A, B, C data were obtained, compared to 2.77nT for CHAMP. Overall, the *Swarm* data seems very well suited for geomagnetic field modelling, and we had no hesitation in using field models based on *Swarm* version 0301/0302 L1b magnetic field data to construct our IGRF-12 candidate models.

CHAOS-5 provides evidence of a secular acceleration pulse around 2013 at the core surface. This amplitude of this new 2013 pulse appears to be larger than the 2009 pulse, and in the Atlantic sector of the core surface its spatial pattern is well correlated to the 2006 pulse, and anti-correlated to 2009 pulse (see also [Chulliat *et al.*, 2015](#)). If another pulse happens around 2016 then *Swarm* will be ideally placed to provide a much more detailed characterization of these presently poorly understood core field pulses.

The CHAOS-5 model, and Matlab software to evaluate it, is available from:
www.spacecenter.dk/files/magnetic-models/CHAOS-5/.

Acknowledgements

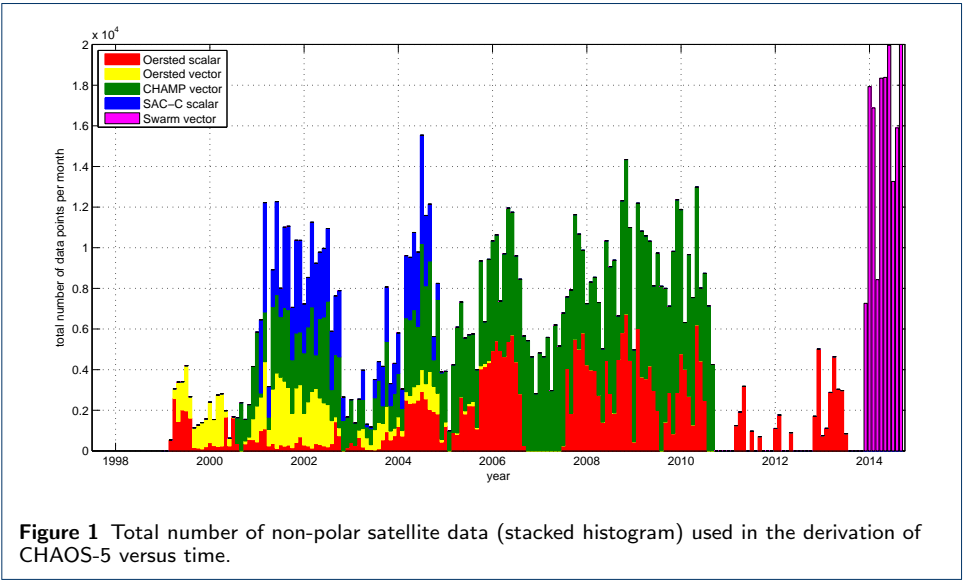
We wish to thank Benoit Langlais, an anonymous reviewer, and the guest editor Erwan Thébault for constructive comments that helped us to improve the manuscript. ESA are thanked for providing prompt access to the *Swarm* L1b data. The staff of the geomagnetic observatories and INTERMAGNET are thanked for supplying high-quality observatory data, and BGS are thanked for providing us with checked and corrected observatory hourly mean values. The support of the CHAMP mission by the German Aerospace Center (DLR) and the Federal Ministry of Education and Research is gratefully acknowledged. The Ørsted Project was made possible by extensive support from the Danish Government, NASA, ESA, CNES, DARA and the Thomas B. Thriges Foundation.

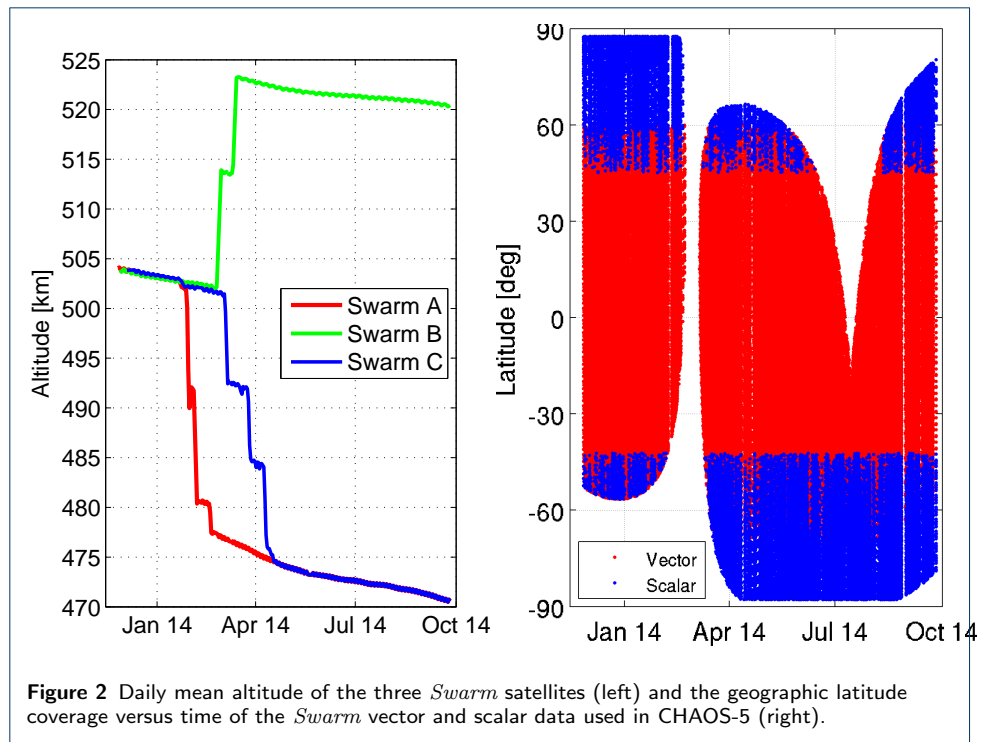
References

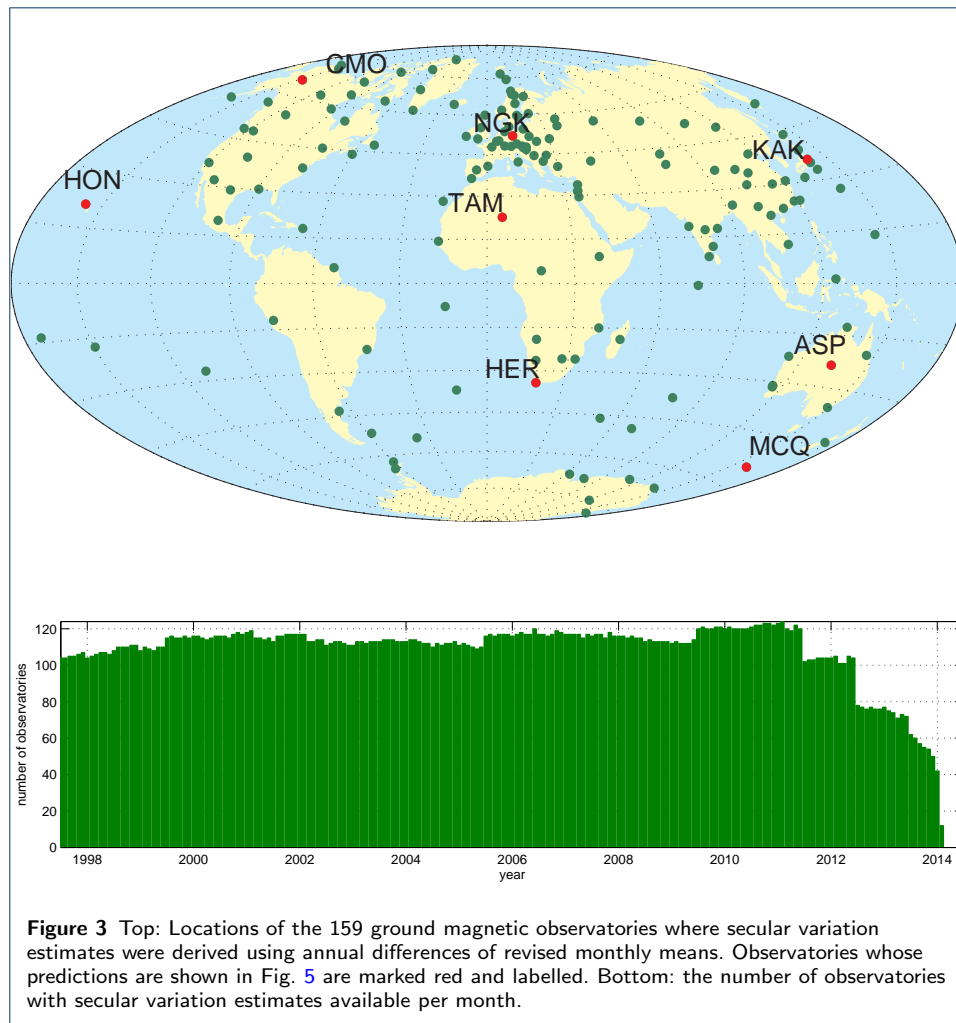
- Chulliat, A., and S. Maus (2014), Geomagnetic secular acceleration, jerks, and a localized standing wave at the core surface from 2000 to 2010, *J. Geophys. Res.*, **119**, doi:10.1002/2013JB010604.
- Chulliat, A., E. Thébault, and G. Hulot (2010), Core field acceleration pulse as a common cause of the 2003 and 2007 geomagnetic jerks, *Geophys. Res. Lett.*, **37**, doi:10.1029/2009GL042019.
- Chulliat, A., P. Alken, and S. Maus (2015), Fast equatorial waves propagating at the top of the Earth's core, *Geophys. Res. Lett.*, p. doi:10.1002/2015GL064067.
- De Boor, C. (2001), A practical guide to splines, *Applied Mathematical Sciences*, **27**.
- Finlay, C. C., S. Maus, C. D. Beggan, T. N. Bondar, A. Chambodut, T. A. Chernova, A. Chulliat, V. P. Golovkov, B. Hamilton, M. Hamoudi, R. Holme, G. Hulot, W. Kuang, B. Langlais, V. Lesur, F. J. Lowes, H. Lühr, S. Macmillan, M. Manda, S. McLean, C. Manoj, M. Menvielle, I. Michaelis, N. Olsen, J. Rauberg, M. Rother, T. J. Sabaka, A. Tangborn, L. Tøffner-Clausen, E. Thébault, A. W. P. Thomson, I. Wardinski, Z. Wei, and T. I. Zvereva (2010), International Geomagnetic Reference Field: The eleventh generation, *Geophys. J. Int.*, **183**, 1216–1230.
- Gillet, N., D. Jault, and C. C. Finlay (2015), Planetary gyre and time-dependent mid-latitude eddies at the Earth's core surface, *J. Geophys. Res.*, p. doi:10.1002/2014JB011786.
- Holme, R., and J. Bloxham (1996), The treatment of attitude errors in satellite geomagnetic data, *Phys. Earth Planet. Int.*, **98**, 221–233.
- Huber, P. J. (1964), Robust estimation of a location parameter, *Ann. Math. Statist.*, **35**, 73–101.
- Lesur, V., I. Wardinski, M. Rother, and M. Manda (2008), GRIMM: the GFZ Reference Internal Magnetic Model based on vector satellite and observatory data, *Geophys. J. Int.*, **173**, 382–294.
- Lesur, V., M. Rother, I. Wardinski, R. Schachtschneider, M. Hamoudi, and A. Chambodut (2015), Parent magnetic field models for the IGRF-12 GFZ-candidates, *Earth, Planets and Space*, **67**, doi:10.1186/s40623-015-0239-6.
- Lowes, F. J. (2000), An estimate of the errors of the IGRF/DGRF fields 1900 – 2000, *Earth, Planets and Space*, **52**, 1207–1211.
- Macmillan, S., and N. Olsen (2013), Observatory data and the Swarm mission, *Earth, Planets and Space*, **65**, 1355–1362.
- Maus, S., C. Manoj, J. Rauberg, I. Michaelis, and H. Lühr (2010), NOAA/NGDC candidate models for the 11th generation International Geomagnetic Reference Field and the concurrent release of the 6th generation Pomme magnetic model, *Earth, Planets and Space*, **62**, 729–735.
- Newell, P. T., T. Sotirelis, K. Liou, C.-I. Meng, and F. J. Rich (2007), A nearly universal solar wind-magnetosphere coupling function inferred from 10 magnetospheric state variables, *J. Geophys. Res.*, **112**, doi: 10.1029/2006JA012015.
- Olsen, N. (2002), A model of the geomagnetic field and its secular variation for epoch 2000 estimated from Ørsted data, *Geophys. J. Int.*, **149**(2), 454–462.
- Olsen, N., and M. Manda (2008), Rapidly changing flows in the Earth's core, *Nature Geoscience*, **1**(6), 390–395.
- Olsen, N., R. Holme, G. Hulot, T. Sabaka, T. Neubert, L. Tøffner-Clausen, F. Primdahl, J. Jørgensen, J.-M. L  ger, D. Barraclough, J. Bloxham, J. Cain, C. Constable, V. Golovkov, A. Jackson, P. Kot  z  , B. Langlais, S. Macmillan, M. Manda, J. Merayo, L. Newitt, M. Purucker, T. Risbo, M. Stampe, A. Thomson, and C. Voorhies (2000), Ørsted Initial Field Model, *Geophys. Res. Lett.*, **27**, 3607–3610.
- Olsen, N., H. L  hr, T. J. Sabaka, M. Manda, M. Rother, L. T  ffner-Clausen, and S. Choi (2006), CHAOS – a model of Earth's magnetic field derived from CHAMP, Ørsted, and SAC-C magnetic satellite data, *Geophys. J. Int.*, **166**, 67–75.
- Olsen, N., M. Manda, T. J. Sabaka, and L. T  ffner-Clausen (2009), CHAOS-2 – A Geomagnetic Field Model Derived from one Decade of Continuous Satellite Data, *Geophys. J. Int.*, **179**(3), 1477–1487.
- Olsen, N., M. Manda, T. J. Sabaka, and L. T  ffner-Clausen (2010), The CHAOS-3 Geomagnetic Field Model and Candidates for the 11th Generation of IGRF, *Earth, Planets and Space*, **62**, 719–727.
- Olsen, N., E. Friis-Christensen, R. F  lberghagen, P. Alken, C. D. Beggan, A. Chulliat, E. Doornbos, J. T. da Encarnac  , B. Hamilton, G. Hulot, J. van den IJssel, A. Kuvshinov, V. Lesur, H. L  hr, S. Macmillan, S. Maus, M. Noja, P. E. H. Olsen, J. Park, G. Plank, C. Puette, J. Rauberg, P. Ritter, M. Rother, T. J. Sabaka, R. Schachtschneider, O. Sirol, C. Stolle, E. Thebault, A. W. P. Thomson, L. T  ffner-Clausen, J. Velimsky, P. Vigneron, and P. N. Visser (2013), The Swarm Satellite Constellation Application and Research Facility (SCARF) and Swarm Data Products, *Earth, Planets and Space*, **65**, 1189–1200.
- Olsen, N., H. L  hr, C. C. Finlay, and L. T  ffner-Clausen (2014), The CHAOS-4 Geomagnetic Field Model, *Geophys. J. Int.*, **197**, 815–827.
- Rother, M., V. Lesur, and R. Schachtschneider (2013), An algorithm for deriving core magnetic field models from the Swarm data set, *Earth, Planets and Space*, **65**, 1223–1231.

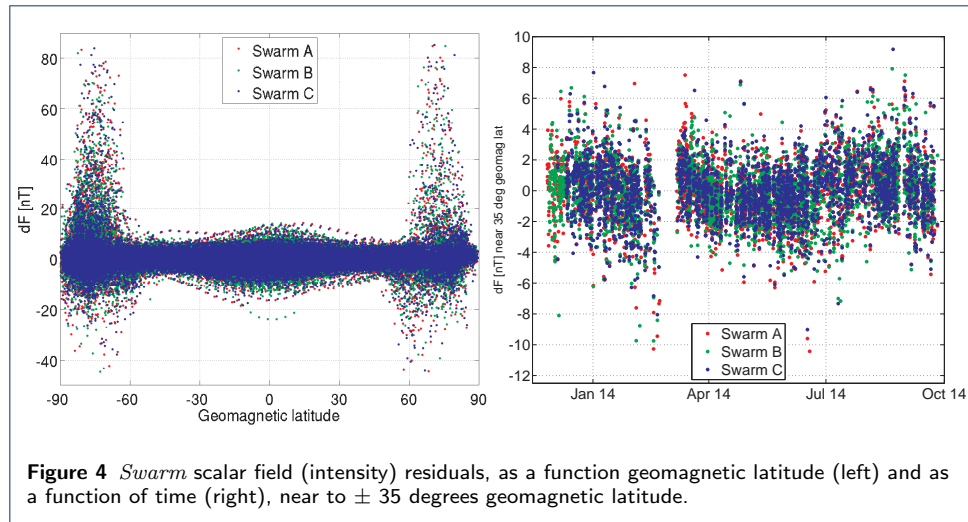
- 486 Sabaka, T. J., N. Olsen, and M. E. Purucker (2004), Extending comprehensive models of the Earth's magnetic field
487 with Ørsted and CHAMP data, *Geophys. J. Int.*, *159*, 521–547.
- 488 Sabaka, T. J., N. Olsen, R. Tyler, and A. Kuvshinov (2015), CM5, a pre-Swarm comprehensive magnetic field model
489 derived from over 12 years of CHAMP, Ørsted, SAC-C and observatory data, *Geophys. J. Int.*, *200*, 1596–1626.
- 490 Thébaud, E., C. C. Finlay, P. Alken, C. Beggan, A. Chulliat, E. Canet, B. Langlais, V. Lesur, F. J. Lowes, C. Manoj,
491 M. Rother, and R. Schachtschneider (2015), Evaluation of candidate geomagnetic field models for IGRF-12,
492 *Earth, Planets and Space*, *67*, in press.
- 493 Thomson, A., B. Hamilton, S. Macmillan, and S. Reay (2010), A novel weighting method for satellite magnetic data
494 and a new global magnetic field model, *Geophys. J. Int.*, *181*, 250–260.

495 **Figures**









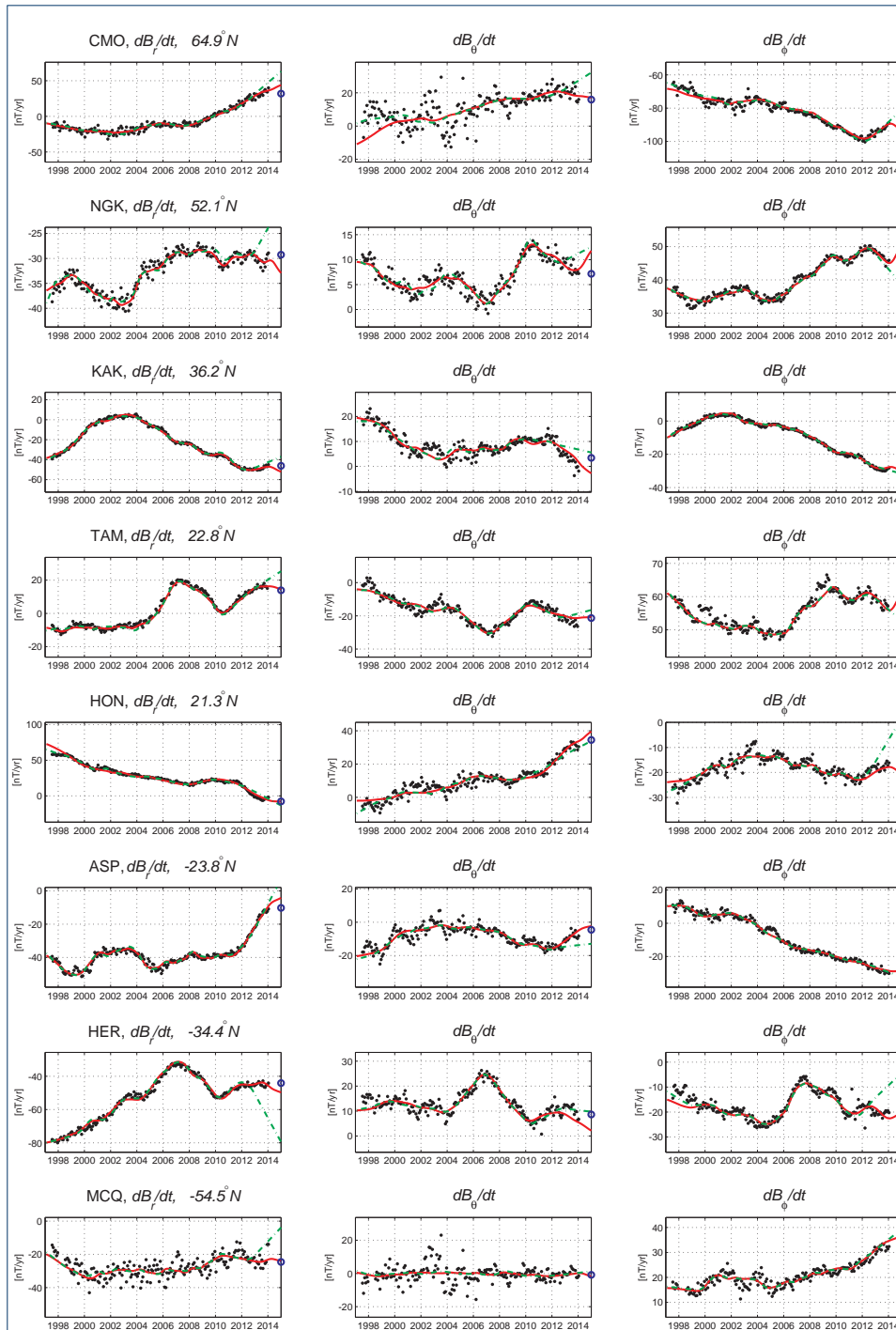
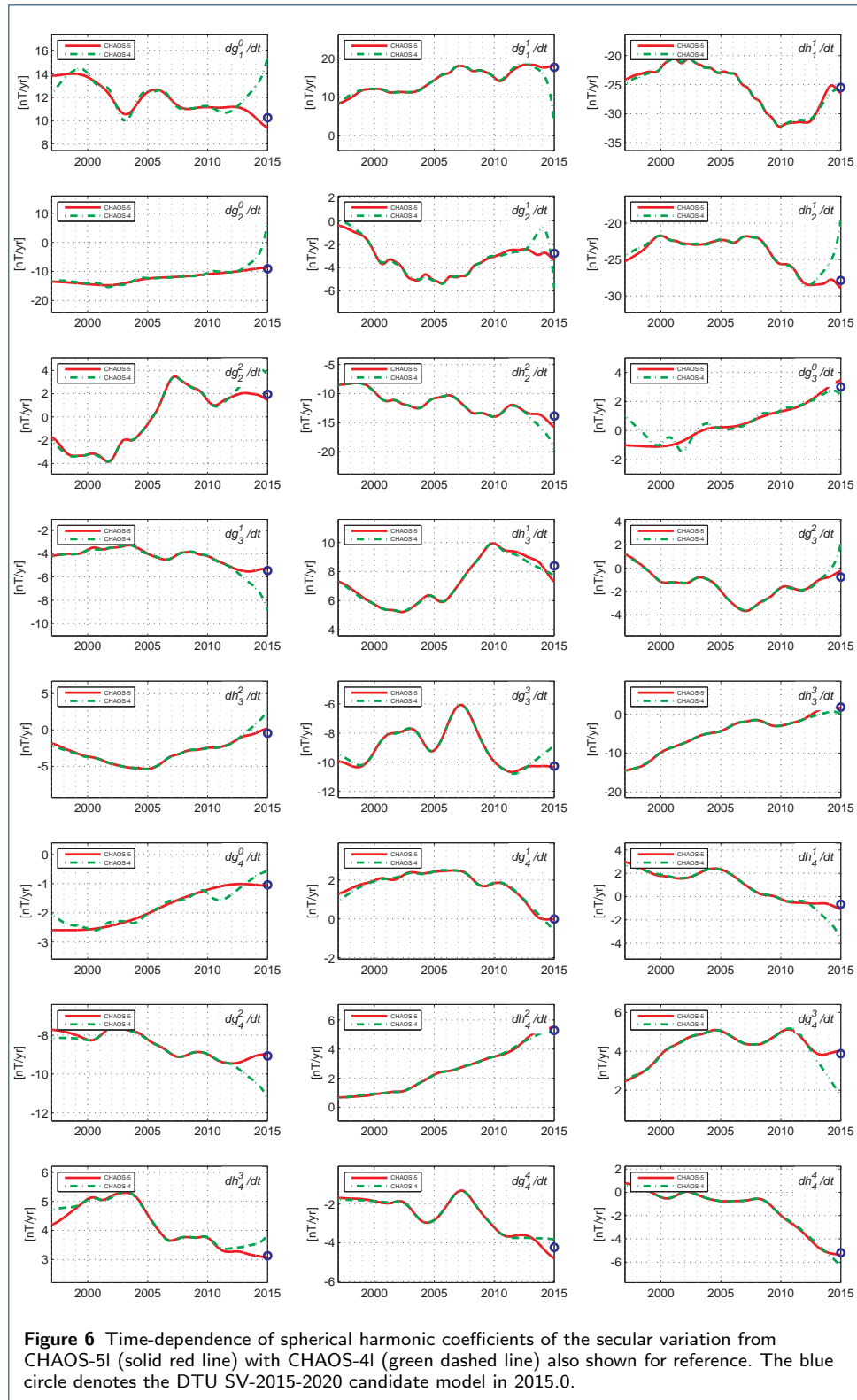
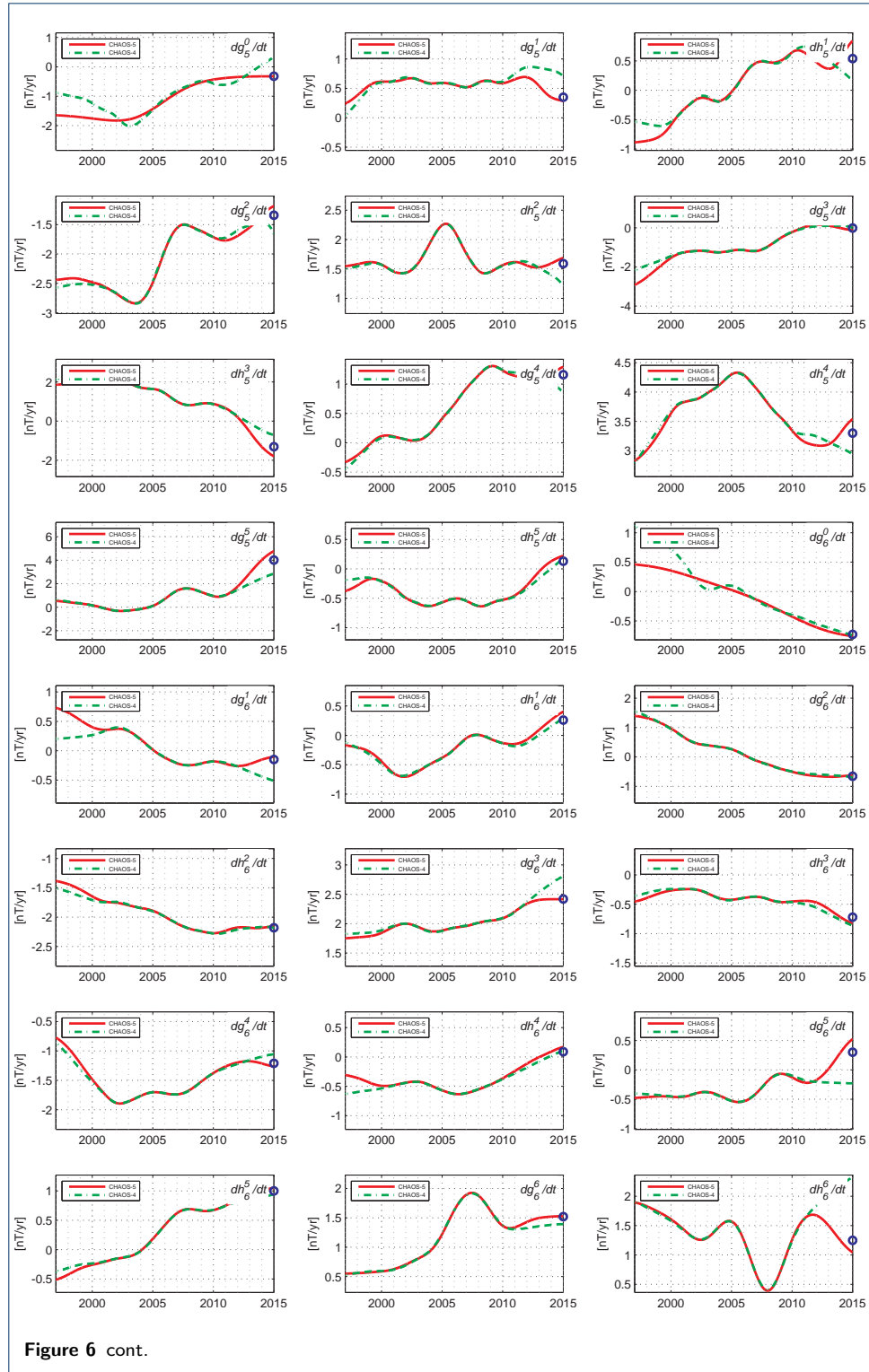
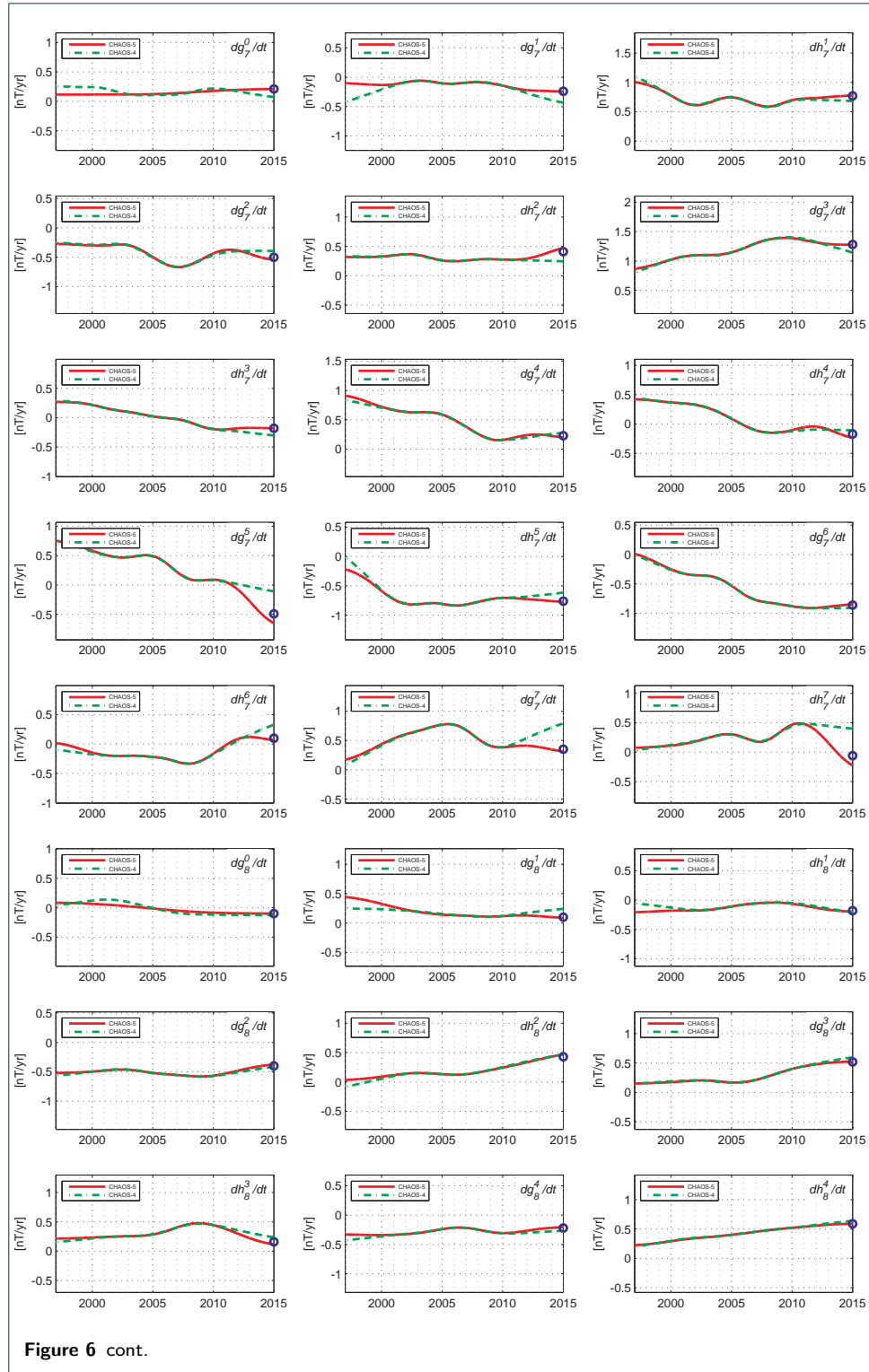
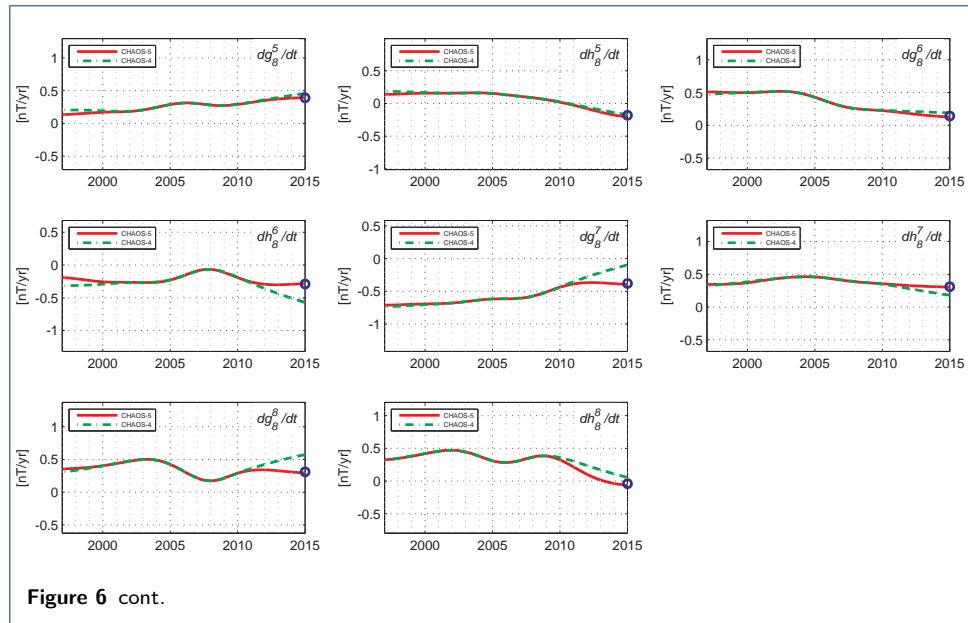


Figure 5 Annual differences of observatory revised monthly means (black dots) compared to the SV predictions from CHAOS-5I (solid red line), those from CHAOS-4I (green dashed line), and for the DTU SV candidate for IGRF-12 (blue circle, shown in 2015.0). For selected observatories, with locations marked in red in Figure 3, arranged by geographic latitude and with field components in the geomagnetic dipole frame.









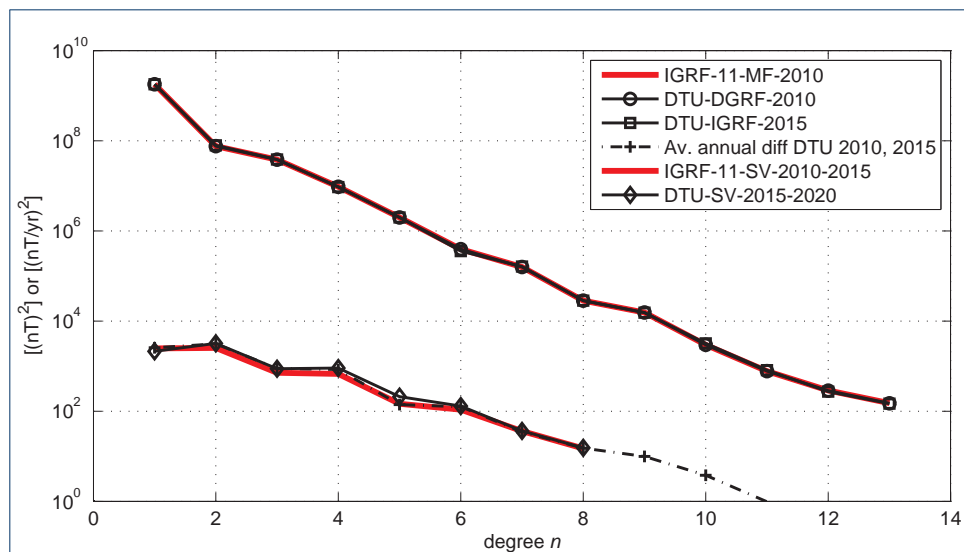
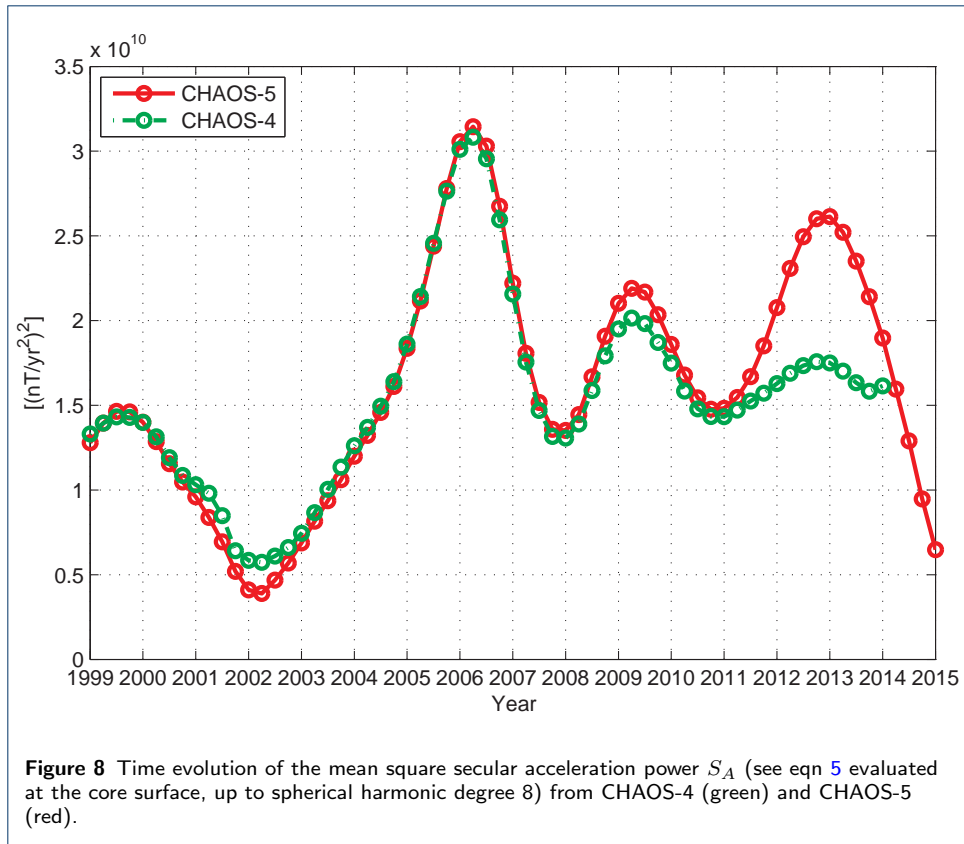
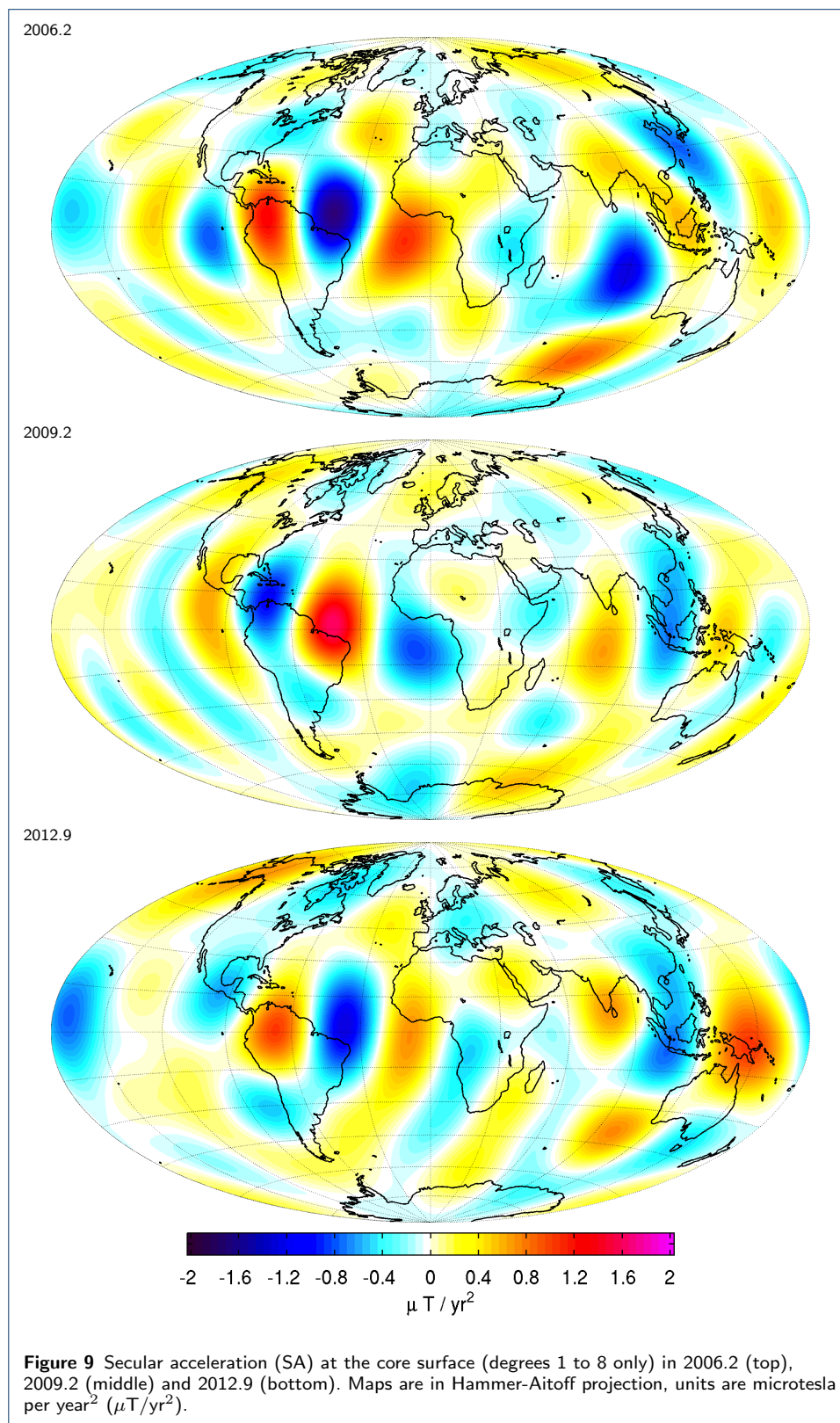


Figure 7 Power spectra at the Earth's surface of the DTU candidate models for IGRF-12 (i) DGRF candidate for the MF in epoch 2010.0 (black line with circles); (ii) IGRF candidate for the MF in epoch 2015.0 (black line with squares) and (iii) candidate for the predicted linear SV 2015-2020 (black line with diamonds). Also shown is the average annual change between the DTU MF candidate models in 2010.0 and 2015.0 (black dashed line with crosses) as well as the IGRF-11 MF model for epoch 2010.0 and the IGRF-11 predicted SV 2010.0-2015.0 (both red lines).





496 Tables

Table 1 Comparison of the CHAOS-4 and CHAOS-5 geomagnetic field models. Contributing data, model parameterization, and model regularization are presented. Improvements of CHAOS-5 compared to CHAOS-4 are shown in bold. $\langle \rangle$ indicates integration over the core-mantle boundary.

	CHAOS-4	CHAOS-5
Data Sources		
Observatory monthly means	June 1997-June 2013	June 1997- Sept 2014
Ørsted vector	March 1999-Dec 2004	March 1999-Dec 2004
Ørsted scalar	March 1999-June 2013	March 1999-June 2013
SAC-C scalar	Jan 2001-Dec 2004	Jan 2001-Dec 2004
CHAMP vector & scalar	Aug 2000 -Sept 2010	Aug 2000 - Sept 2010
<i>Swarm A</i> vector & scalar	-	Nov 2013 - Sept 2014
<i>Swarm B</i> vector & scalar	-	Nov 2013 - Sept 2014
<i>Swarm C</i> vector & scalar	-	Nov 2013 - Sept 2014
Time-Dependent Internal Field		
Model time span	1997.0-2013.5	1997.0 - 2015.0
Spherical harmonic degree	$n = 1 - 20$	$n = 1 - 20$
Spline basis	6th order, 0.5yr knots	6th order, 0.5yr knots
Based on	CHAOS-4l	CHAOS-5l
Static Internal Field		
Spherical harmonic degree	$n = 21 - 90$	$n = 21 - 90$
Based on	CHAOS-4l ($n = 21 - 24$) & CHAOS-4h ($n = 25 - 90$)	CHAOS-5l ($n = 21 - 24$) & CHAOS-4h ($n = 25 - 90$)
External Field		
SM	$n = 1$: 1hr, RC int + ext 5day Δq_1^0 , 30 day Δq_1^1 , Δs_1^1	$n = 1$ 1hr, RC int + ext 5day Δq_1^0 , 30 day Δq_1^1 , Δs_1^1
GSM	$n = 2$: static $n = 1 - 2$, $m = 0$	$n = 2$: static $n = 1 - 2$, $m = 0$
Euler Angles		
Ørsted	before & after Jan 24th 2000	before & after Jan 24th 2000
CHAMP	10 day bins	10 day bins
<i>Swarm</i>	-	10 day bins
Regularization		
Spatial	static field $n > 85$, $\langle B_r^2 \rangle$ $\lambda_0 = 1 \text{ nT}^{-2}$	static field $n > 85$, $\langle B_r^2 \rangle$ $\lambda_0 = 1 \text{ nT}^{-2}$
Temporal, interior	$\langle (dB_r^3/dt^3)^2 \rangle$ $\lambda_3 = 0.33 (\text{nT/yr}^{-3})^{-2}$ except g_1^0 , $\lambda_3 = 10 (\text{nT/yr}^{-3})^{-2}$	$\langle (dB_r^3/dt^3)^2 \rangle$ $\lambda_3 = 0.33 (\text{nT/yr}^{-3})^{-2}$ except m=0, $\lambda_3 = 100 (\text{nT/yr}^{-3})^{-2}$
Temporal, endpoints	$\langle (dB_r^2/dt^2)^2 \rangle$ $\lambda_2 = 10 (\text{nT/yr}^{-2})^{-2}$	$\langle (dB_r^2/dt^2)^2 \rangle$ $\lambda_2 = 100 (\text{nT/yr}^{-2})^{-2}$

Table 2 Number of data points N , and the Huber-weighted mean and rms misfits (in nT for the satellite data, and in nT/yr for the ground observatory data) of the data to the CHAOS-5I parent field model. Statistics for the vector components are given both in the coordinate system (B_B, B_\perp, B_3) that is defined by the bore-sight of the star camera and the ambient field direction cf. (Olsen et al., 2000) and also in the standard geocentric (ECEF) frame (B_r, B_θ, B_ϕ) .

	Data	Component	CHAOS-5I		
			N	mean	rms
	Ørsted	F_{polar}	121,293	0.46	3.44
		$F_{\text{nonpolar}} + B_B$	367,713	0.16	2.37
		B_\perp	87,672	-0.05	7.37
		B_3	87,672	0.15	3.35
		B_r	87,672	0.13	4.47
		B_θ	87,672	0.23	5.36
		B_ϕ	87,672	0.00	5.03
	CHAMP	F_{polar}	188,015	-0.37	4.90
		$F_{\text{nonpolar}} + B_B$	497,394	-0.09	2.07
		B_\perp	497,394	-0.02	3.30
		B_3	497,394	0.07	3.42
		B_r	497,394	0.02	2.77
		B_θ	497,394	0.10	3.56
		B_ϕ	497,394	-0.01	2.71
	SAC-C	F_{polar}	26,118	0.43	3.78
		F_{nonpolar}	86,603	0.40	2.72
	Swarm A	F_{polar}	17,485	-0.03	3.80
		$F_{\text{nonpolar}} + B_B$	53,137	-0.01	2.09
		B_\perp	53,137	-0.05	2.79
		B_3	53,137	0.05	2.72
		B_r	53,137	-0.01	1.83
		B_θ	53,137	0.18	2.95
		B_ϕ	53,137	-0.16	2.69
	Swarm B	F_{polar}	17,774	0.15	3.65
		$F_{\text{nonpolar}} + B_B$	53,253	-0.06	2.07
		B_\perp	53,253	-0.03	2.80
		B_3	53,253	0.08	2.84
		B_r	53,253	-0.02	1.99
		B_θ	53,253	0.22	3.00
		B_ϕ	53,253	-0.13	2.71
	Swarm C	F_{polar}	16,697	0.13	3.82
		$F_{\text{nonpolar}} + B_B$	49,984	0.05	2.09
		B_\perp	49,984	-0.05	2.80
		B_3	49,984	0.04	2.80
		B_r	49,984	0.02	1.93
		B_θ	49,984	0.11	3.00
		B_ϕ	49,984	-0.15	2.71
	observatory	dB_r/dt	21,733	0.13	3.91
		dB_θ/dt	21,733	-0.02	3.83
		dB_ϕ/dt	21,733	-0.00	3.12